Characterizing-water seepage damage in the chest-abdomen area of the Leshan Giant Buddha

Sun Bo [i], Zhang Peng [ii], Shen Xiwang [iii] and Liu Yuyuan [iiii]

i) Ph.D Student, Department of Civil Engineering, Lanzhou University, Rd 222 South Tianshui, Lanzhou, Gansu, China.
ii) Assistant Engineer, Northwest Research Institute Co., Ltd. of C. R. E.C, Rd 365 East Mingzhu, Lanzhou, Gansu, China.
iii) Mid-level Engineer, Northwest Research Institute Co., Ltd. of C. R. E.C, Rd 365 East Mingzhu, Lanzhou, Gansu, China.
iiii) Mid-level Engineer, Leshan Giant Buddha Management Committee Museum, Rd 2435 Lingyun, Leshan, Sichuan, China.

ABSTRACT

The water seepage damage in the chest-abdomen area of the Leshan Giant Buddha is significant, which causes the sandstone in the body of the Buddha to corrode and crack, makes the repair materials on the surface of the Buddha hollow and desquamate, and leads to the growth of biological damage. In this study, continuous monitoring and sampling of the water seepage in the chest-abdomen area of the Leshan Giant Buddha and the atmospheric precipitation were performed. The water seepage in the chest-abdomen area of the Buddha is primarily controlled by atmospheric precipitation and evaporation. The hysteresis effect of water seepage reflects that the bedrock fissure on the left is relatively developed with significant water transmissibility. During the atmospheric precipitation monitoring period, the average pH of atmospheric precipitation was 8.13, i.e., weakly alkaline. After 2009, the annual average pH of atmospheric precipitation for the Buddha was greater than 5.6 and increased year by year. The water seepage of the Buddha contained a large amount of ions. The chemistry type of water seepage in the chest-abdomen ares is calcium carbonate ($CaCO_3$) and calcium sulfate ($CaSO_4$). Rock weathering contributes more than 90% of the ions in the Buddha water seepage. The microscopic analysis of the rock shows that the main components of the rock are $CaCO_3$ and SiO_2, and there is obvious layered morphology, is easy to be dissolved in the presence of air and water. The composition of water chemical ions indicates that H_2CO_3 and H_2SO_4 are both involved in the process of the weathering of the sandstone.

Keywords: atmospheric precipitation, Leshan Giant Buddha, seepage damage, weathering

1 INTRODUCTION

The Leshan Giant Buddha (also known as Lingyun Giant Buddha) is located in Leshan City, Sichuan Province, where the Minjiang River, Qingyi River and Dadu River converge. The Buddha, built in the first year of Emperor Xuanzong (AD 713) and completed in the 19th year of Emperor Dezong (AD 803), is one of the finest works of art in the field of inscriptions on precipices of the Tang Dynasty and the largest stone statue of Maitreya Buddha in the world. In December 1996, the Emeishan-Leshan Giant Buddha was listed as World Natural and Cultural Heritage Site by the United Nations Educational, Scientific and Cultural Organization.

The ancients excavated three drainage tunnels in the head, neck and chest of the Buddha, which cut off the influence of water seepage on the head to some extent. Since modern times, the restoration and protection of Leshan Giant Buddha has been ongoing, but the seepage damage has not been solved. The Buddha's chest-abdomen is the area where the surface water seeps down and the upper layer water seeps out. The rock stratum in this section has been in the state of seepage, which not only causes dissolution and cracking of the sandstone in the body of the Buddha, but also makes the repair materials on the surface of the Buddha hollow, damaged and crack, and leads to the growth of biological damage in the Buddha's body (Fig. 1).

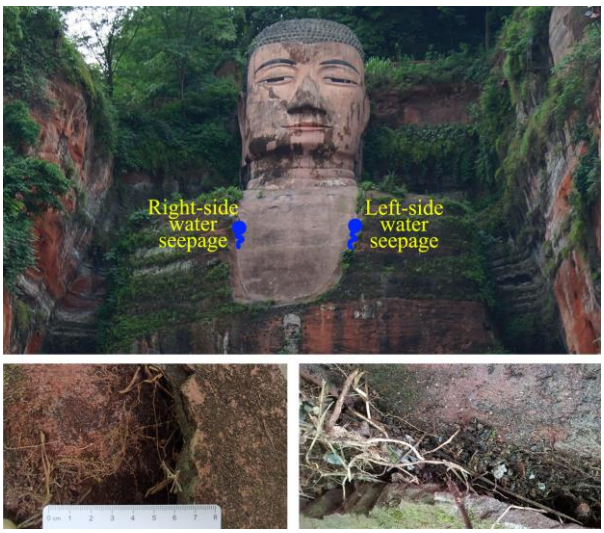

Fig. 1. Leshan Giant Buddha and water seepage damage.

The authors systematically monitored the water seepage in the chest-abdomen of Leshan Giant Buddha (the left and the right) and the atmospheric precipitation there, analyzed the sources and chemistry of the Buddha's water seepage, and studied the weathering mechanism of the Buddha sandstone via the hydrochemistry and microscopic composition of rock. The protection of cultural relics from water damage has been difficult historically. Qin Zhong et al. (2005) studied the weathering rate and erosion mechanism of the Leshan Giant Buddha sandstone, and found that biological and water erosion invasion were the two primary factors contributing to the weathering damage of the rock carvings. Siegesmund et al. (2014) studied the performance and durability of historic stone, and analyzed the behavior of the rocks under wet-dry cycling and subjected to the effect of water and salts. Shaojun et al. (2013) performed out a degradation simulation test on the sandstone of the Yungang Grottoes, and noted that the development of soluble salts is an important factor that leads to the pulverization and desquamate damage. Mingshen et al. (2015) studied the weathering mechanism of the sandstone cultural relics in Chengde Mountain Resort, and noted that the dissolution of calcareous cement, wet-dry cycling, and the expansion of salt crystallization are the primary reasons for the sandstone pulverization and desquamate.

2 MONITORING AND ANALYSIS METHODS

This study monitored the water seepage in the chest-abdomen area of the Buddha during the normal season (April), the wet season (July) and the dry season (December) in 2019, and atmospheric precipitation were monitored from 28 to 30 in July 2019. Atmospheric precipitation was collected by using a simple rain gauge, and the water seepage was collected by leading the seepage down to the Buddha's feet through a drainage pipe. The pH, electrical conductivity (*EC*) and total dissolved solids (TDS) of water samples were field tested using a Leici Portable Multi-Parameter Water Quality Analyzer (Model: DZB-71). The cations were measured by inductively coupled plasma-optical emission spectrometry or ICP-OES (Model: Optima 5300 DV) and the anions were measured by ion chromatography (Model: ICS 2100). At the same time, x-ray diffraction (XRD), X-ray fluorescence (XRF) and scanning electron microscopy (SEM) were used to analyze the rock composition and microstructure of the cliff.

During the sampling process, water seepage in the chest-abdomen was sampled hourly in dry weather, whereas water seepage and precipitation were sampled every 15 min when there was precipitation. 25 rainwater samples and 103 water seepage samples were collected during the monitoring period (47 from the left and 56 from the right). During the monitoring period, the primary atmospheric precipitation started at 20:40 on July 28 2019 and lasted 22h 50min. The accumulated atmospheric precipitation was 116.0 mm.

3 TEMPORAL-SPATIAL DISTRIBUTION OF ATMOSPHERIC PRECIPITATION AND WATER SEEPAGE

3.1 Influencing factors of water seepage

In April, the water seepage for the left-side ranged from 20 to 185 mL/h, with an average of 108 mL/h. From the Fig. 2, it can be seen that the water seepage volume changes regularly with time. The water seepage volume increases continuously from 17:00 to 07:00 every day, from 07:00 to 17:00 water seepage continues to decrease. April is in a normal season, the atmospheric precipitation is low, and the amount of water seepage is primary affected by evaporation. During the day 07:00-17:00, the amount of ground evaporation is high, and the amount of water seepage decreases; at night 07:00-17:00, the amount of ground evaporation decreases. Smaller, the amount of water seepage increases. In addition, the water seepage can still maintain a stable and regular change under the conditions of low atmospheric precipitation, indicating that groundwater is the primary source of replenishment for seepage during normal season.

In July, the water seepage for the left-side ranged from 0 to 2300 mL/h, with an average value of 26 mL/h. The water seepage for the right-side ranged from 0 to 2880 mL/h, with an average value of 57 mL/h. The surface evaporation in July was high, and the amount of seepage in dry weather was approximated to 0 mL/h. Due to the high evaporation, the shallow groundwater was significantly affected, and the water seepage did not show a daily regular change in July (Fig. 3). July is in the wet season; atmospheric precipitation is concentrated and the amount of precipitation is high. Water seepage increased in the presence of precipitation was significantly higher with some exceeding 2000 mL/h.

In December, the water seepage for the left-side ranged from 0 to 83 mL/h, with an average value of 2 mL/h. The right water seepage ranged from 0 to 42 mL/h, with an average value of 2 mL/h. December is in the dry season, and the water seepage is very low compared with April and July. Evaporation has a certain influence on the amount of water seepage. In December, the daily seepage volume shows a certain regular change. The water seepage is the smallest at 20:00, and largest at 12:00 (Fig. 4).

During normal and dry season, the primary source of water seepage in the chest-abdomen area of the Buddha is groundwater, and during the wet season, due to the high evaporation, it has a significant impact on the shallow groundwater. The seepage occurs in the presence of precipitation. The primary source of water seepage is atmospheric precipitation, and the rock under the cycling of dry and wet. Due to the influence of evaporation during normal and dry season, the water seepage changes regularly every day.

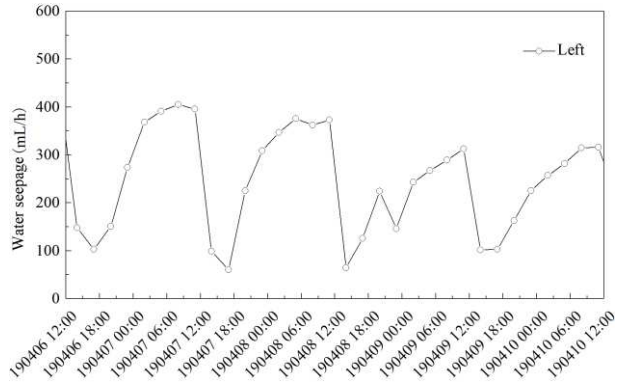

Fig. 2. Water seepage(April 6 - 8, 2019).

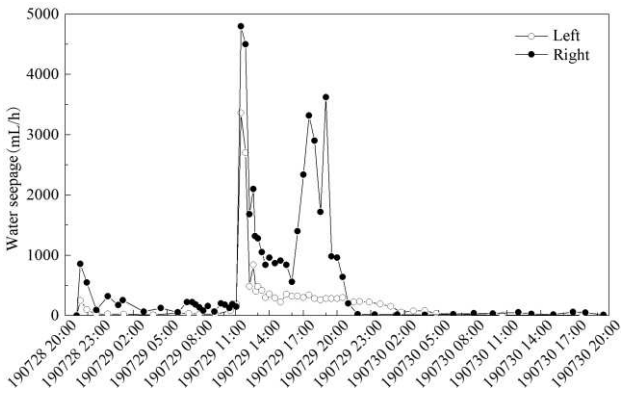

Fig. 3. Water seepage (July 28 - 30, 2019).

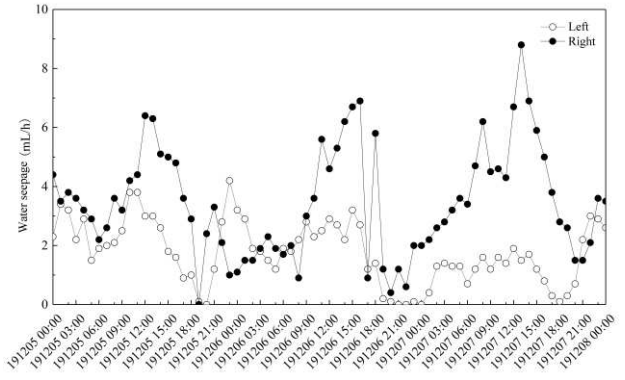

Fig. 4. Water seepage (December 5～8, 2019).

Table 1 Monthly average temperature and radiation in April, July and December 2019

Time	April	July	December
Temperature (℃)	19.8	24.7	10.0
Radiation (rad/24h)	133	176	85

In July 2019, water seepage and atmospheric precipitation in the chest-abdomen area of the Buddha were sampled systematically. The first atmospheric precipitation period began at 08:50 on July 27, at 15:20 on the same day, water seepage occurred in the left of the Buddha, with the seepage lagging the atmospheric precipitation by 5.5 h, and no water seepage occurred in the right. The second atmospheric precipitation period began at 20:40 on July 28, and the chest-abdomen of the Buddha began to seep at 21:00 on the same day. The atmospheric precipitation intensity and water seepage over time during the second atmospheric precipitation period (Fig. 5) shows consistent correlations between the atmospheric precipitation intensity and the water seepage. The peak of water seepage for the left lags the peak of atmospheric precipitation intensity by 48 min, and the primary peak of water seepage for the right lags the peak of atmospheric precipitation intensity by 73 min.

The hysteresis in the water seepage for the chest-abdomen area of the Buddha for both light rain and storm event shows that the fissures in the left bedrock are more developed, the water transmissibility is high, and the atmospheric precipitation is discharged quickly through the bedrock fissure. The amount of water seepage from the right is higher than that from the left, which may be due to the large atmospheric precipitation catchment area on the right of the Buddha and the large amount of groundwater recharge provided by atmospheric precipitation. Under the two atmospheric precipitation conditions, in addition to the primary first peak, there are two obvious secondary peaks for the right water seepage, i.e., the second and third peaks. These second and third peaks lag the atmospheric precipitation peaks by 7h and 9h, which indicates that the internal structure of the right rock of the Buddha is complicated. The right water seepage receives atmospheric precipitation recharge from three different sources, two of which have longer seepage channels.

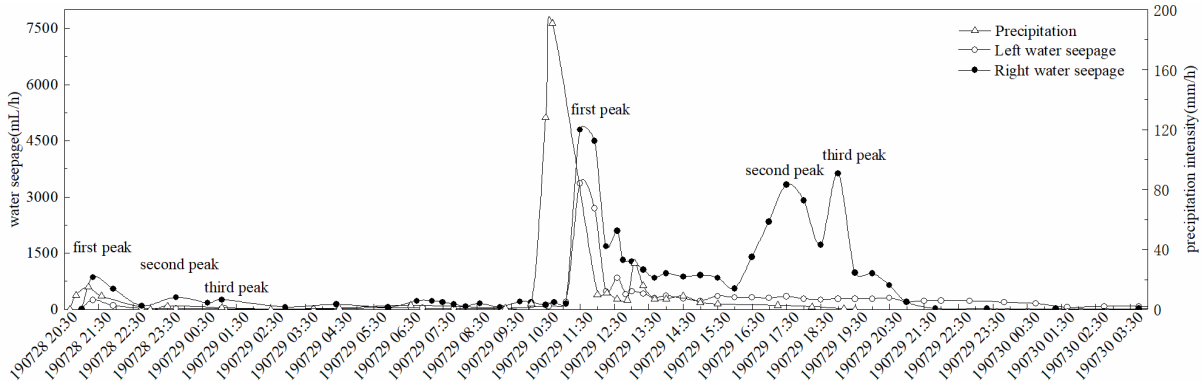

Fig. 5. Precipitation intensity and water seepage over time.

3.2 The pH

The pH is one of the most important environmental factors that determines the migration and transformation of chemical elements in water. The average atmospheric precipitation pH during the monitoring period was 8.13, which is weakly alkaline. Leshan from 1991 to 2017 (Fig. 6), the atmospheric precipitation in the Leshan Giant Buddha area has gradually changed to weakly alkaline, compared with the acid rain (pH <5.6) in earlier years, indicating that acid rain has been effectively controlled.

During the monitoring period, the pH of atmospheric precipitation was high and ranged from 7.47 to 8.97. Generally, there are two primary reasons for the high pH, i.e., the lack of acid ions (NO_3^- and SO_4^{2-}), and the introduction of alkaline substances that neutralized the acidic conduction (Calvofernandez et al. 2017, Liu et al. 2017). Data from the Huahuwan Air Quality Monitoring Station shows that, in July of 2019, the concentrations of SO_2 and NO_2 in the atmosphere at Leshan were the lowest for the entire year, and the precipitation caused acid ions deficiency (Fig. 7.). The release of NH_3 and other alkaline compounds produced by agricultural activities such as planting wheat and rice provides a possible source of alkalinity for the atmospheric precipitation. The agricultural activities in summer are frequent, and the application of nitrogen fertilizers over a large area will release ammonia nitrogen into the atmosphere in the form of NH_3, which generates NH_4^+ that increase the pH in the atmospheric precipitation.

During the monitoring period, the average pH for the left and right water seepages were 7.70 and 7.72 (Fig. 8), which are not significantly different. Compared to water seepage in the chest-abdomen areas, the pH of the atmospheric precipitation is more alkaline. The pH of the water seepage increases over time and then stabilizes (Fig. 9). During atmospheric precipitation, the pH of the initial water seepage for the left and the right are close to 7.0. However, with time, the water seepages pH increases towards that for the atmospheric precipitation, and finally stabilizes at about 8.0 after about 22 h.

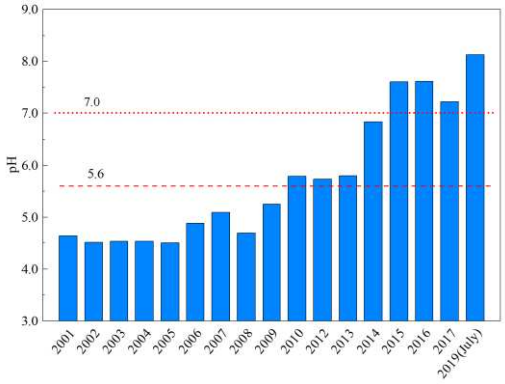

Fig. 6. pH of the Leshan Giant Buddha over the years. (1991-2000 refer to Zhou Junyi, 2004; 2001-2003 refers to Daining et al. 2004; 2004-2008 refers to Yuanqiong et al. 2015; 2009-2017 refers to Bureau of Ecology Environment of Le Shan).

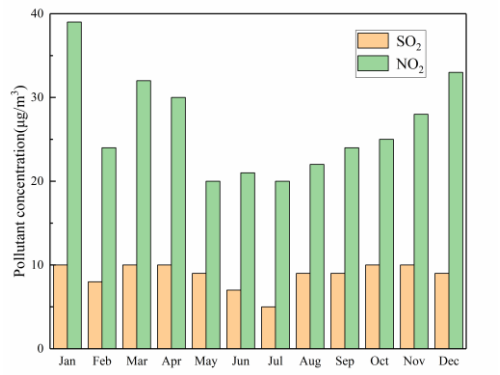

Fig. 7. SO_2 and NO_2 in the atmosphere in 2019.

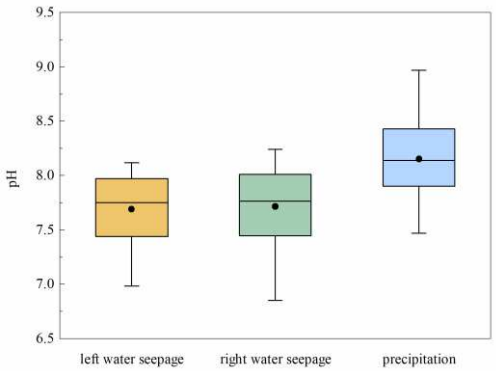

Fig. 8. Variation range of pH value.

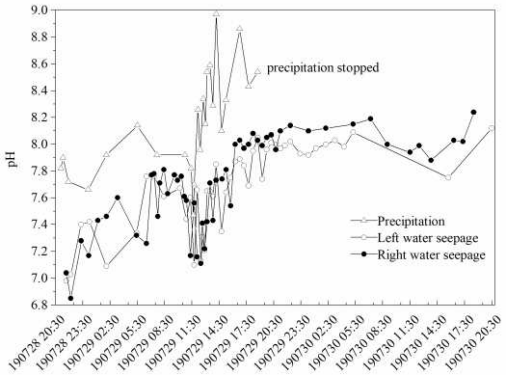

Fig. 9. pH value change over time.

3.3 *EC* and TDS

The *EC* is an indicator of the contribution of ions in water, and to a certain degree reflects the length of the water cycle and the residence time (Xianfang et al. 2006). The average *EC* of the atmospheric precipitation, left-side water seepage and right-side water seepage were 2 mS/m, 117.8 mS/m, and 76.3 mS/m (Fig. 10). The *EC* in the chest-abdomen area of the Buddha was 40 to 60 times greater than that for the atmospheric precipitation, indicating that water seepage in the chest-abdomen of the Buddha stayed longer in the bedrock, and the water seepage contained a large amount of ions. The *EC* for the left side was greater than that for the right side, indicating more dissolved ions in the left side.

The TDS is a measurement of the contribution of ions

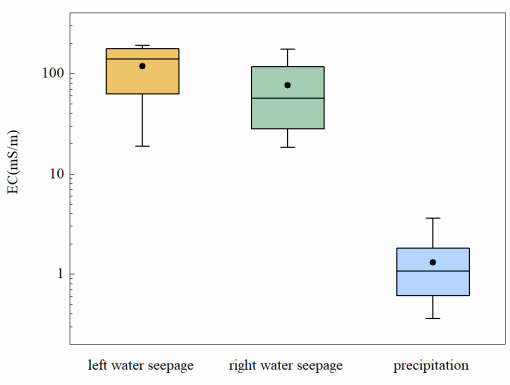

Fig. 10. Variation in EC.

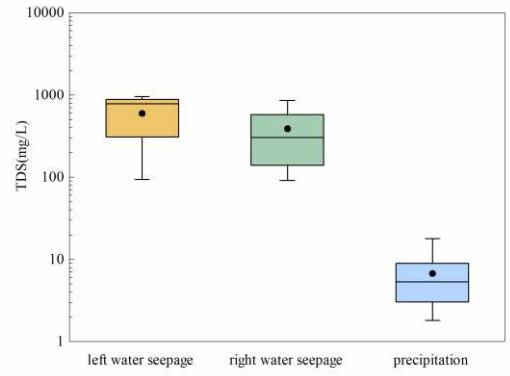

Fig. 11. Variation in TDS.

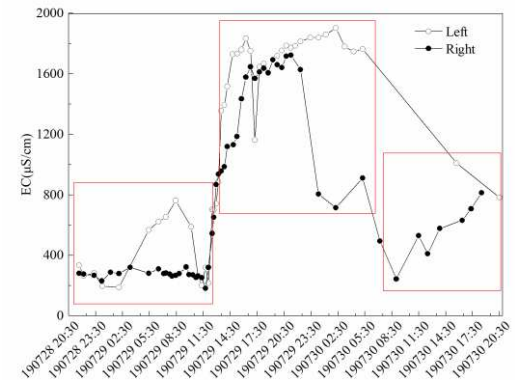

Fig. 12. Temporal variation in EC of water seepage.

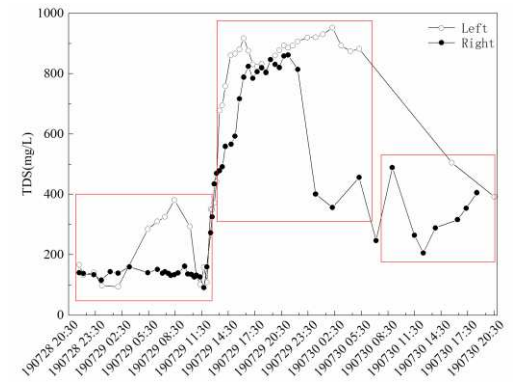

Fig. 13. Temporal variation in TDS of water seepage.

dissolved in water, which can reflect the lithology, soil, vegetation, weathering erosion rate, and human activities to a certain extent. The average TDS of the atmospheric precipitation, left-side, and right-side were 19.5 mg/L, 594.1 mg/L and 387.7 mg/L, respectively (Fig. 11). The TDS of atmospheric precipitation was low, and the TDS in the chest-abdomen area of the Buddha was 20-30 times greater than that of atmospheric precipitation, which indicates that the atmospheric precipitation has a strong dissolution capacity on the bedrock during the seepage-flow-drainage process. Consistent with the *EC* value, the TDS for the left side is higher than that for the right side.

The temporal changes in the *EC* and TDS of the water seepage in the chest-abdomen area of the Buddha shown in Fig. 9 and Fig. 10, respectively, and the curve of TDS are basically consistent. According to the curve in EC and TDS value, the water seepage in the chest-abdomen area of the Buddha can be divided into the early, middle and late period (Fig. 12, Fig. 13). The early period water seepage contained a small number of ions, which may be the previous several atmospheric precipitations that was stranded near the seepage point of the Buddha. As the atmospheric precipitation caused the pressure of the vadose increase, the water near the seepage point was the priority to exude. The water seepage in the middle period was the previous atmospheric precipitation stored in the bedrock fissure of the Buddha. Because the storage time is long and the flow path is long in the Buddha, a large number of soluble bedrock components are dissolved and exuded under the promotion of this atmospheric precipitation. The later period water seepage contained a small number of ions, which means that the atmospheric precipitation mixed with the previous atmospheric precipitation reached the outlet, and EC and TDS value began to show a downward trend.

3.4 Hydrochemical

Calcium (Ca^{2+}) accounts for 70% of the total cation equivalents dissolved in the water seepage associated with the chest-abdomen area of the Buddha. In general, the abundance of the cations in the seepage water is in the order $Ca^{2+} > Na^{+} > Mg^{2+} > K^{+}$, whereas is the abundance of anions is in the order $SO_4^{2-} > HCO_3^{-} > Cl^{-} > NO_3^{-}$, with SO_4^{2-} and HCO_3^{-} contributing 59% and 22% of the anions, respectively. Except for Cl^{-}, The temporal variations in ion concentrations shown in Fig.14 mimic those for EC and TDS as previously discussed, which were low in the initial and latter periods and high during the middle period.

According to Aleksin's Classification, the water seepage in the early and late periods is primarily dominated with $CaCO_3$ m, i.e., Type II water, whereas the water seepage in the middle period is primarily $CaSO_4$, i.e., Type III water. Type II water has a medium or low degree of mineralization, which is affected by water and sedimentary rocks. Type III water generally has a high degree of mineralization and the ion exchange

action in water causes the water composition to change significantly.

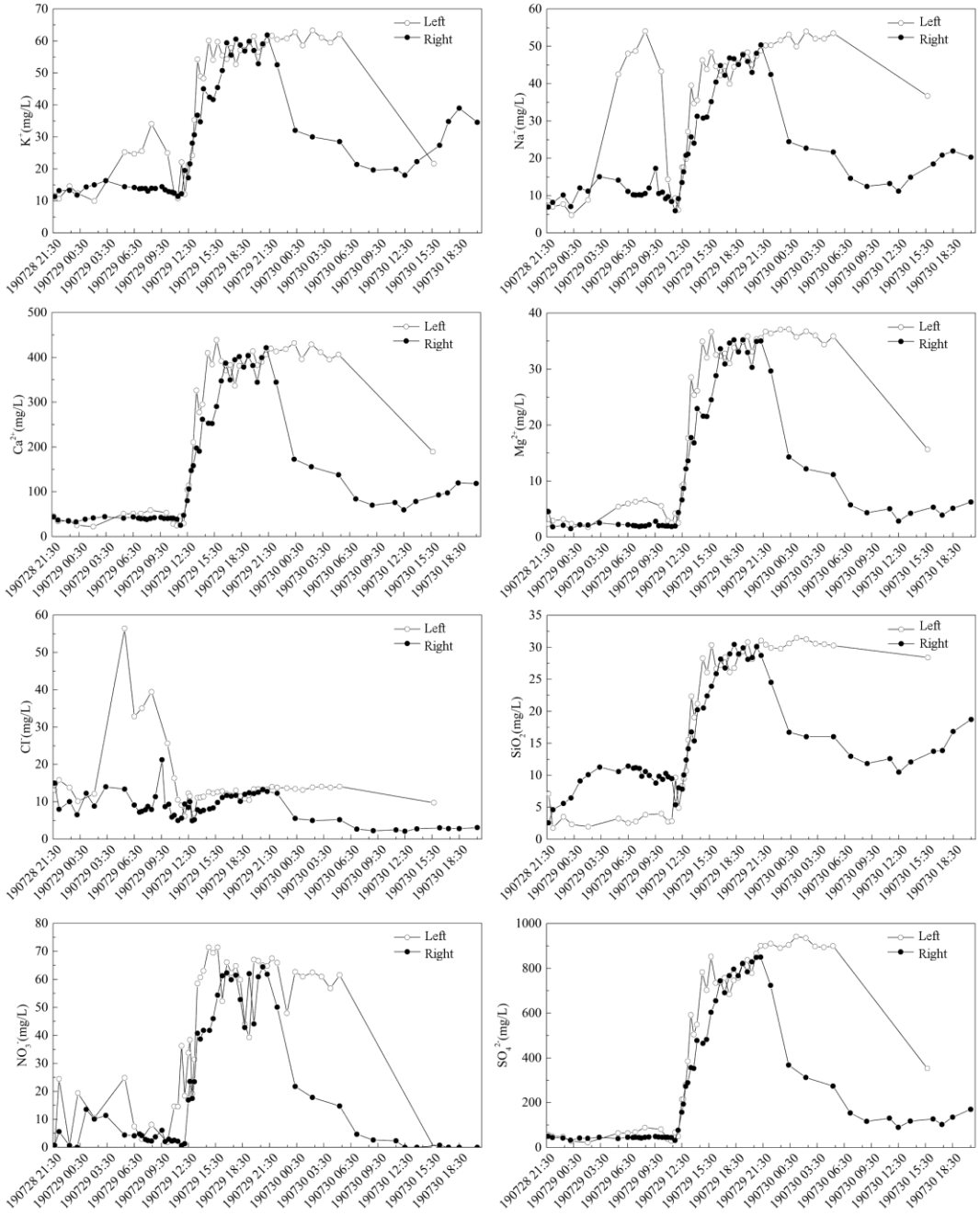

Fig. 14. The contribution of each ion in the water seepage change over time.

3.5 Ions sources in water seepage

Leshan Giant Buddha Scenic Spot has a beautiful environment and strict management. There is almost no anthropogenic pollution in the area that affects the chemical composition of the water seepage. Therefore, the chemical composition of water seepage in the chest-abdomen area of the Buddha is primarily derived from atmospheric precipitation and rock dissolution. Chloride(Cl^-) is the primary component in the atmospheric precipitation, and is more conservative, not easily adsorbed, and difficult to settle, and the concentration is very low in the rock and does not participate in the biogeochemical cycle (Moon et al.,2007; Xu et al., 2007). Chloride is usually used as a reference element to analyze the influence of atmospheric precipitation on the chemical composition of water body, and the contribution of other meteoric input elements can be obtained by comparing the ratio of Cl^- to other elements in atmospheric precipitation and the Cl^- input of meteoric atmospheric precipitation in water body. Calculated as follows:

$$[Cl^-]_{atm} = \frac{P}{(P-E)\times(Cl^-)_{ref}} \quad (1)$$

Where: $[Cl^-]_{atm}$. represents the Cl^- contribution input

to the water body by atmospheric precipitation, $(Cl^-)_{ref}$. represents the average contribution of Cl^- in the atmospheric precipitation (reference), *P* represents the average annual atmospheric precipitation (atmospheric precipitation; mm), and *E* represents the average evaporation (mm) for many years. The summer atmospheric precipitation is referenced from China Meteorological Administration, and the evaporation is referenced from Linyun et al. (2017).

From the result of the analysis, the source of ions in the water seepage of the Buddha is primarily rock weathering (over 90% in general). Atmospheric precipitation has some effect on NO_3^- and HCO_3^-, but has little effect on other ions (<10%).

Table 2. Contribution of atmospheric precipitation and rock weathering to seepage ion. (Note: 0 represents ion contribution is lower than the detection limit)

Ions	Ca^{2+}	K^+	Mg^{2+}	Na^+	Cl^-	NO_3^-	HCO_3^-	SO_4^{2-}
Water seepage(mmol/L)	19.92	0.88	2.72	1.24	1.19	1.80	1.07	19.00
Atmospheric Perception (mmol/L)	0.034	0	0	0.028	0.033	0.018	0.031	0.132
Contribution of precipitation (%)	1	0	0	6	9	14	11	4
Contribution of rock weathering (%)	99	100	100	94	91	86	89	96

3.6 Water-rock interaction

The Buddha sandstone is the lower layer of the lower Cretaceous System jiaguan formation (*K2j*). Samples of the sandstone were recovered from the left cliff at the elevation of the chest-abdomen area of the Buddha and analyzed (see Fig. 15). Five sampling points were designed according to the height, and each sampling point was sampled at different depths (depth B: 0－2 cm, C: 2－4 cm, D: 4－6cm).

The XRD results (shown in Fig. 16) indicate that the primary ingredient is quartz with some calcite small amounts of kaolinite and muscovite.

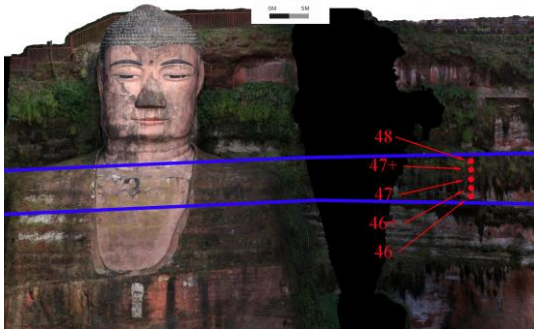

Fig. 15. Rock sampling locations.

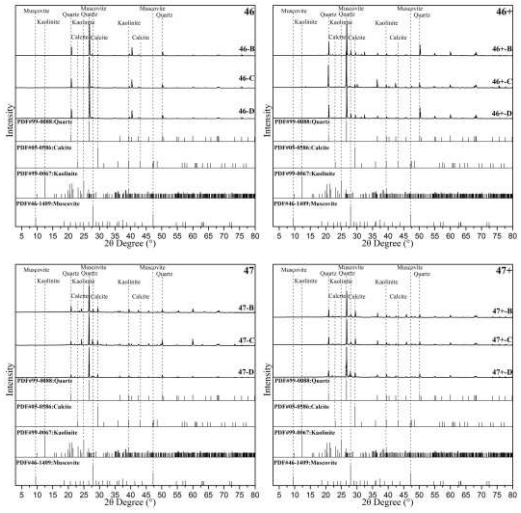

Fig. 16. X-ray diffraction (XRD) results.

Analysis results of XRF of the rock (Table 3) show that the primary composition of the rock is SiO_2 (> 50%), with some CaO and Al_2O_3 (> 8%), and a smaller amount of MgO, Na_2O, K_2O and Fe_2O (< 4%). Considering that SiO_2 is stable in air and water, only the change in $CaCO_3$ was mainly analyzed. The content of $CaCO_3$ in the rock samples at the middle and upper part (numbered 47, 47+ and 48) was low, such that the loss of $CaCO_3$ was significant. During groundwater leakage, $CaCO_3$ collected at the lower rock stratum. The middle and upper strata have the lowest $CaCO_3$ content at C: 2－4 cm and were strongly affected by weathering.

The SEM analysis of the rock samples (Fig. 17) shows that many particles were distributed on the surface of the bedrock, and the fractures were all granular, with particle sizes ranging from a few microns to several hundred microns. The entire structure is dense, the surface is rough, micro-cracks had not developed, and occasionally there are holes and caverns. The surface morphology of each layer is not different from that shown by the low power SEM images. High power SEM images (5000 times) shows that the microstructure of the rock samples is granular or massive, irregular in shape, with good cementation, relatively dense in some locations with obvious micro-fractures, irregular and multi-caverns. The particles of 38B exhibited obvious layered morphology, which has a large specific surface area and is more prone to corrosion in the presence of air and water.

Table 3. X-Ray Fluorescence (%).

Samples	SiO_2	CaO	Al_2O_3	MgO	Na_2O	K_2O	Fe_2O
46-B	55.41	13.28	9.87%	2.08	1.46	1.96	2.59
46-C	56.32	15.25	8.85	2.75	2.65	1.45	2.32
46-D	56.32	15.25	8.85	2.75	2.65	1.45	2.32
46+B	49.53	15.06	9.81	2.77	1.54	1.69	2.73
46+C	52.35	13.16	10.54	2.26	1.60	1.89	2.94
46+D	52.54	13.52	10.28	2.02	1.63	1.78	3.08
47-B	55.84	10.15	12.03	3.78	1.51	2.26	3.35
47-C	50.36	9.99	14.31	2.75	1.45	1.79	2.85
47-D	59.49	10.39	8.85	2.98	1.53	2.08	2.98
47+B	55.08	10.65	11.61	3.14	1.51	2.06	3.53
47+C	55.09	10.65	11.61	3.14	1.51	2.06	3.59

47+D	54.36	11.45	10.67	3.08	1.55	2.11	3.72
48-B	55.62	11.49	10.29	2.04	1.57	1.86	2.66
48-C	55.09	10.65	11.61	3.14	1.51	2.06	3.53
48-D	54.36	10.67	11.45	3.08	1.55	2.11	3.72

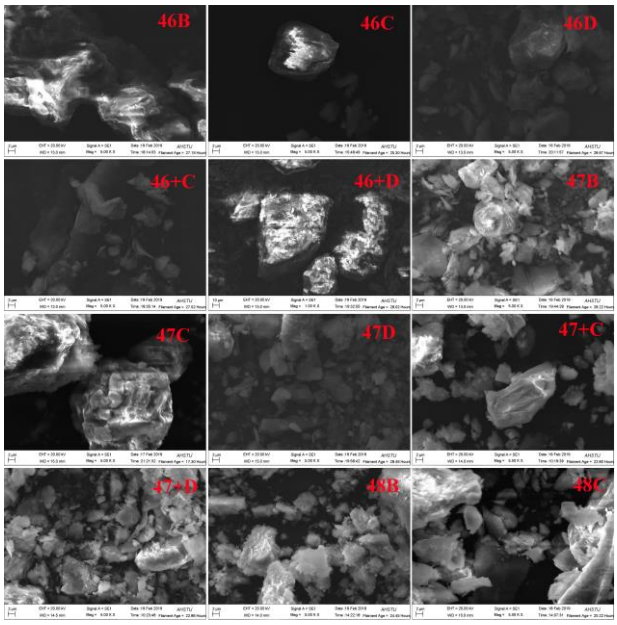

Fig. 17. Scanning Electron Microscope.

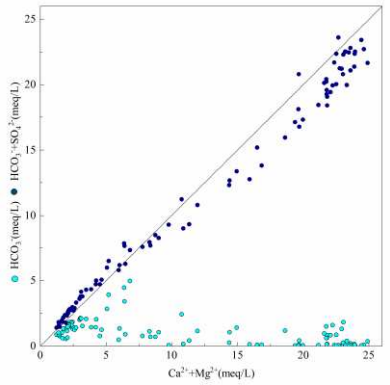

Fig. 18. (Ca^{2+} + Mg^{2+}) versus (HCO_3^- + SO_4^{2-}) for the water seepage.

The weathering products of rocks largely determined the hydrochemical properties of groundwater. Generally speaking, CO_2 from atmosphere or soil is the most common erosion medium for chemical weathering of carbonate rocks, and H_2SO_4 is generally involved in the weathering process of rocks (Spence et al., 2005; Zhang et al., 2015). The chemical weathering process of HCO_3 and H_2SO_4 can be simplified as follow:

$$C_{a_x}Mg_{1-x}CO_3 + CO_2 + H_2O \rightarrow xC_a{}^{2+} + (1-x)Mg^{2+} + 2HCO_3^- \quad (2)$$

$$2C_{a_x}Mg_{1-x}CO_3 + H_2SO_4 \rightarrow 2xC_a{}^{2+} + 2(1-x)Mg^{2+} + 2HCO_3^- + SO_4{}^{2-} \quad (3)$$

When H_2CO_3 participates in weathering, the weathering products of carbonate rocks are mainly Ca^{2+}, Mg^{2+} and HCO_3^-, and the equivalent ratio of (Ca^{2+} + Mg^{2+}) / HCO_3^- should be unity. However, the equivalent ratio of (Ca^{2+} + Mg^{2+})/HCO_3^- in the seepage of the Buddha is much higher than this, indicating that HCO_3^- ion alone is not enough to balance with Ca^{2+} and Mg^{2+}.The primary anion in the seepage is SO_4^{2-}, which accounts for 59% of the total anion equivalent, and is derived primarily from the atmospheric input of SO_2 and the oxidation of sulfide minerals. Figure. 18 shows the (Ca^{2+} + Mg^{2+})/(HCO_3^- + SO_4^{2-}) equivalent ratio of the seepage. When H_2SO_4 participates in the reaction, the equivalent ratio of (Ca^{2+} + Mg^{2+})/(HCO_3^- + SO_4^{2-}) is basically unity, indicating that H_2SO_4 is involved in the weathering of the Buddha sandstone and plays an important role.

4 CONCLUSIONS

The main sources of water seepage in the chest-abdomen area of Leshan Giant Buddha are groundwater and atmospheric precipitation, and the amount of water seepage is controlled by atmospheric precipitation and evaporation. The hysteresis effect of water seepage shows that the fissures of the left side are more developed and the water transmissibility is more predominant, and the right side water seepage is recharged by atmospheric precipitation from three different sources.

The average pH value of atmospheric precipitation during the monitoring period was 8.13, which was weakly alkaline. The annual average pH of atmospheric precipitation in Leshan City is higher than 5.6 since 2009, and higher than 7 in 2015. The average pH of water seepage in the chest-abdomen area is 7.70, which increased first and then stabilized. The average TDS is 19.5 mg/L of atmospheric precipitation, 594.1 mg/L for the left-side water seepage, and 387.7 mg/L for the right-side water seepage. The average EC is 2 mS/m for the atmospheric precipitation, 117.8 mS/m for left-side water seepage, 76.3 mS/m for the right-side water seepage. In the process of seepage flow and drainage, there is obvious dissolution on the bedrock, and the left-side water seepage dissolves the rock more strongly.

The chemistry of water seepage in the chest-abdomen area of the Buddha is calcium carbonate (Type II) and calcium sulfate (Type III). The cations are primary Ca^{2+}, accounting for 70% of the equivalent sum of cations. The primary anions were SO_4^{2-} and HCO_3^-, accounting for 59% and 22% of the total cation equivalent. The contribution of rock weathering to ions in the water seepage of the Buddha is more than 90%, and the contribution of atmospheric precipitation which influences the NO_3^- and HCO_3^- concentrations.

The primary mineral constituents of the Buddha sandstone are $CaCO_3$ and SiO_2. The microscopic analysis indicates that the rocks in the chest-abdomen area of the Buddha have layered morphology and are prone to dissolution in the presence of air and water. The hydrochemical ion composition analysis indicates that H_2CO_3 and H_2SO_4 participate in the weathering of the

Buddha sandstone.

REFERENCES

1) Cheng, Y. Q. and Ou, S. (2015): Analysis on the trend and causes of acid rain pollution in Leshan Giant Buddha Scenic Spot, *Annual meeting of Chinese society for environmental science*, Shenzhen, China, 1139-1142. (in Chinese)
2) Calvofernandez, J., Marcos, E. and Calvo, L. (2017): Bulk deposition of atmospheric inorganic nitrogen in mountainous heathland ecosystems in North-Western Spain, *Atmospheric Research*, 183, 237-244.
3) Gao, L. Y., Huang, X. R., Xi, Y. Y., Li, J. J. and Ma, K. (2017): Analysis of temporal and spatial distribution characteristics of climate change in Sichuan basin based on cloud model, *Journal of North China University of Water Resources and Electric Power (Natural Science Edition)*, 38(01), 1-7. (in Chinese)
4) Liu, X. Y., Xiao, H. W., Xiao, H. Y., Song, W., Sun, X. C., Zheng, X. D., Liu, C. Q. and Koba, K. (2017): Stable isotope analyses of precipitation nitrogen sources in Guiyang, southwestern China, *Environmental Pollution*, 230, 486-494.
5) Moon, S., Huh, Y., Qin, J. and Van Pho, N. (2007): Chemical weathering in the Hong (Red) River basin: Rates of silicate weathering and their controlling factors, *Geochimica et Cosmochimica Acta*, 71(6), 1411-1430.
6) Qin, Z., Zhang, J., Peng, X.Y. and Wang, X. S. (2005): A study on weathering processes of Leshan Giant Buddha, Sichuan, China, *Geographical Research*, 6, 928-934. (in Chinese)
7) Shao, M. S., Zhang, Z. J. and Li, L. (2015): Properties and deterioration mechanism of sandstone blocks in Chengde royal buildings between 1703 and 1792, *Journal of engineering geology*, 23(03), 533-538. (in Chinese)
8) Shu, D. N. and Deng, X. F. (2007): Study on acid deposition and control measures of Leshan Giant Buddha Scenic Spot, a world heritage site, *China sustainable development forum and China sustainable development academic annual conference*, Beijing, China. (in Chinese)
9) Siegesmund, S. and Akos, T. (2014): Building Stone, Stone in Architecture Properties, Durability 5th Edition, Berlin, Springer-Verlag, 1-552.
10) Spence, J. and Telmer, K. (2005): The role of sulfur in chemical weathering and atmospheric CO_2 fluxes: Evidence from major ions, $\delta^{13}C_{DIC}$, and $\delta^{34}S_{SO4}$ in rivers of the Canadian Cordillera, *Geochimica et Cosmochimica Acta*, 69(23),5441-5458.
11) Song, X. F., Liu, X. C., Xia, J., Yu, J. J. and Tang, C. Y. (2006): A study of interaction between surface water and groundwater using environmental isotope in huaisha river basin, *Science China-earth Sciences*, 49(12), 1299-1310.
12) Xu, Z. F. and Liu, C. Q. (2007): Chemical weathering in the upper reaches of Xijiang River draining the Yunnan-Guizhou Plateau, Southwest China, *Chemical Geology*, 239(1-2),83-95.
13) Yan, S. J., Fang, Y., Liu, J. H. and Tan, S. E. (2013): Deterioration experiment with soluble salt on sandstone of Yungang grottoes and its model creation, *Rock and soil mechanics*, 34(12), 3410-3416. (in Chinese)
14) Zhang, Q. Q., Jin, Z. D., Zhang, F. and Xiao, J. (2015): Seasonal variation in river water chemistry of the middle reaches of the Yellow River and its controlling factors, *Journal of Geochemical Exploration*, 156, 101-113.
15) Zhou, J. Y. (2004): Impact assessment and prevention measures of acid rain on bedrock of Leshan Giant Buddha, *Journal of Leshan Normal University*, 2, 107-110. (in Chinese).